applied sciences

MDPI

Article

Configurable 3D Rowing Model Renders Realistic Forces on a Simulator for Indoor Training

Ekin Basalp [1,*], Patrick Bachmann [1], Nicolas Gerig [2], Georg Rauter [1,2] and Peter Wolf [1]

1 Sensory-Motor Systems Lab, Department of Health Sciences and Technology, Institute of Robotics and Intelligent Systems, ETH Zurich, 8092 Zurich, Switzerland; patricba@student.ethz.ch (P.B.); georg.rauter@unibas.ch (G.R.); peter.wolf@hest.ethz.ch (P.W.)

2 BIROMED-Lab, Department of Biomedical Engineering, University of Basel, 4123 Basel, Switzerland; nicolas.gerig@unibas.ch

* Correspondence: basalp.ekin@hest.ethz.ch

Received: 31 December 2019; Accepted: 17 January 2020; Published: 21 January 2020

Abstract: In rowing, rowers need outdoor and indoor training to develop a proficient technique. Although numerous indoor rowing machines have been proposed, none of the devices can realistically render the haptic, visual, and auditory characteristics of an actual rowing scenario. In our laboratory, we developed a simulator to support rowing training indoors. However, rendered forces with the initial rowing model, which was based on a simplified fluid dynamic model that approximated the drag/lift forces, were not perceived realistic enough for indoor training by expert rowers. Therefore, we implemented a new model for the blade–water interaction forces, which incorporates the three-dimensional rotation of the oar and continuously adjusts drag/lift coefficients. Ten expert rowers were asked to evaluate both models for various rowing aspects. In addition, the effect of individualization of model parameters on the perceived realism of rowing forces was elaborated. Based on the answers of the experts, we concluded that the new model rendered realistically resistive forces and ensured a smooth transition of forces within a rowing cycle. Additionally, we found that individualization of parameters significantly improved the perceived realism of the simulator. Equipped with a configurable rowing model, our simulator provides a realistic indoor training platform for rowers.

Keywords: 3D force modeling; rowing biomechanics; robot-assisted training; individualized training; virtual reality simulator; training of experts; sports engineering; rowing simulator; tendon based parallel robot; transversal vibration control

1. Introduction

In rowing races, success is determined by the minimum time to complete a pre-defined course track of commonly 2000 m [1]. Thus, mathematically, the main performance metric for competitive rowers is the average boat speed to finish the course [2]. Attaining a faster boat speed requires not only a physical effort but also an appropriate boat setup and a skillful technique to transfer the propulsion forces into speed [3–5]. Therefore, fitness and technique trainings are crucial for competitive rowers [5].

Outdoor rowing training may not always be feasible since performance of rowers can be affected by unpleasant weather conditions [6,7]. Indoor training conducted with rowing machines offers a valuable alternative to outdoor practice [8]. Over the past decades, various rowing machines have been developed to yield a realistic rowing training [9]. Overall, the developed machines can be grouped in four categories depending on the technical aspects: indoor rowing tanks, ergometers, ergometer simulators, and virtual reality simulators [10].

For indoor-tank rowing, two large unit water-tanks are used next to a fixed rowing boat [11]. Since the oars directly interact with the real water, the resistance at the oar blade is naturally present. However, water tanks require specially constructed large spaces, which might be challenging to maintain.

Ergometers provide a useful strength training opportunity indoors. On an ergometer, a rower interacts with a handle to simulate the resistance. Rendered resistance is mainly dependent on the pulling speed of the handle. Ergometers generate the desired resistance forces through friction-based interaction of a flywheel with air or water [12]. Since ergometers built with a stationary footrest were found to increase inertial forces and joint injuries compared to the on-water rowing [13], moving footrest systems were also proposed for ergometers such as Rowperfect® Indoor Sculler [14] and Concept2® Dynamic [15]. Thus, the boat's acceleration and deceleration at each stroke can be simulated on such ergometers.

Ergometers do not render the essential kinematic and dynamic characteristics of an oar movement. Thus, advanced ergometer simulators that incorporate the actual handling of a rowing oar with three degrees of freedom were developed [16–18]. In ergometer simulators, rowers manipulate one (sweep) [16] or two shortened oars (sculling) [17] as in the case of actual rowing boats. The rolling motion of an actual boat can also be simulated on ergometer simulators. However, rowing simulators do not incorporate actual water dynamics to render the resistive forces. Resistance is rendered with an air fan and disc brake system, and the resultant force perceived by the rower is mainly dependent on the speed of the oar. Additionally, none of the ergometer simulators provide any visual or auditory displays to bring the realism of the training closer to the on-water rowing experience. Thus, virtual reality simulators were developed to augment the realism of indoor rowing training [19–22].

The virtual rowing training platform SPRINT was developed at Scuola Superiore S.Anna, Pisa, Italy [19,20]. The SPRINT platform included two shortened oars with three degrees of freedom (DoF) each, a fixed foot stretcher, and a sliding seat. Visual rendering of the rowing scenario was coupled to the output of a mathematical model that combined the movement of boat, oars, and a rower. Rendering of hydrostatic vertical forces and oar weight was realized by a mass–spring system. The vertical force model only depended on the vertical rotation of the oar, i.e., the effect of longitudinal rotation of the oar was neglected. Rendering of the horizontal forces in the virtual water was based on a modified form of a dissipation mechanism used in Concept2® ergometers. Due to this mechanism, haptic rendering of the horizontal forces did not capture the fluid-dynamics characteristics of the oar blade–water interaction. Therefore, the haptic rendering of the overall forces in the SPRINT platform was not based on the actual kinematic and dynamic features of a rowing movement.

In our laboratory, we also developed a rowing simulator to support realistic training for sculling and sweep rowing indoors [23]. Thanks to the real-time control and dedicated hardware setup, our rowing simulator has been used for training of rowers [22] and motor learning related research such as augmented feedback designs [24,25] and robotic training strategies [26,27].

The haptic rendering of the rowing forces incorporated the effect of the 3-DoF rotation of an actual rowing oar and of the boat dynamics [28]. The propulsion forces were calculated according to an empirical model [29], which approximated the drag and lift forces acting on the blade [21]. Although the model was previously shown to be suitable for technique training [22], expert rowers suggested that the realism of the rendered resistive forces on the simulator could be improved. Therefore, in this study, we proposed a new three-dimensional force model that incorporates 3-DoF rotation of the oar and accounts for a smooth blade transition between air and water.

The new force model was implemented on our rowing simulator and assessed by ten expert rowers in a training experiment. In the first part of the experiment, rowers were asked to qualitatively assess both the existing oar-blade model [21] and the new model. We hypothesized that the new blade force model would be perceived as more realistic than the existing model. In the second part of the experiment, the benefit of individualizing the force model on expert rowers' acceptance of the rowing

simulator as a training platform was investigated. We hypothesized that the individualization of model parameters would result in higher realism of perceived rowing forces of the simulator.

2. Materials and Methods

2.1. Participants

Ten expert rowers (five females, five males; age = 18–27 years, mean age = 21.8 years; experience of rowing = 5–15 years, mean experience = 7–8 years) were recruited for the experiment. Participants were either students at ETH Zurich and/or affiliated with a rowing club in Zurich or neighboring cities. We set the inclusion criteria for the 'expertness' in rowing as (i) intensive training with port-side sweep rowing for at least 3 years; and (ii) participation in at least one national and one international regatta as a port-side rower.

The current study was approved by the ETH Zurich Ethics Commission (EK 2017-N-75). Each participant was invited for a 2-h session conducted on a single day. Expert participants were verbally instructed about the goal, experimental protocol, assessment by means of a questionnaire, and the potential risks that might occur. In addition, participants were informed that they could withdraw from the study at any time without stating a reason and without facing any consequences. All participants signed a consent for participation and were reimbursed for their commitment with a gift (maximum value of CHF 20).

2.2. Rowing Setup

In the study, our custom-made rowing simulator was used (Figure 1) [21]. The rowing simulator consisted of an instrumented, shortened, single scull boat (Stämpfli Racing Boats AG, Zürich, Switzerland). The boat was placed on a platform in the middle of three 4.4 m × 3.3 m sized screens, i.e., one screen in front of the stern and one screen to each the left and right side of the boat [30].

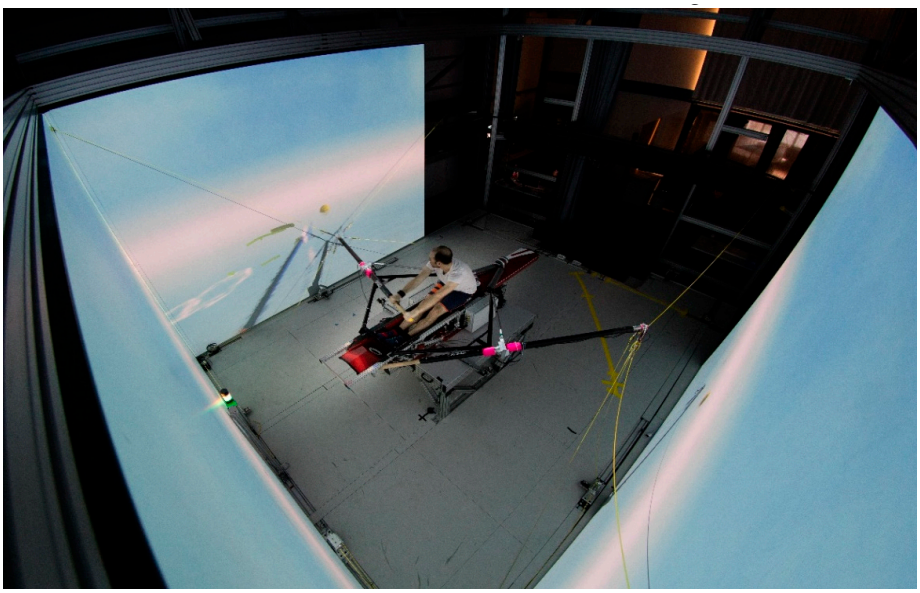

Figure 1. Rowing simulator setup with a shortened single scull boat and three screens surrounding the boat. The person rowing in the boat is the first author of the paper.

A visual scenario representing a plain lake environment along with a line of buoys defining the course was displayed with three projectors (Projection Design F3+) on the large screens. The visual scenario was programmed in Unity (Unity Technologies ApS, CA, USA) and synchronized to the kinematic input from the participant with a minimum update rate of 30 fps.

The auditory rendering of the rowing scenario was developed in C++. Two speakers (DELL A525 Zylux Multimedia Computer Speaker System), which were placed behind the bow of boat, were used to deliver the task inherent, virtual water–oar interaction sounds with an update rate of 30 Hz.

The haptic rendering of the rowing simulator was realized by a tendon-based parallel robot [31]. The robot consisted of five ropes attached to the end-effector, i.e., shortened oar, in parallel, and five actuation units that were placed on a fixed frame [21]. The ropes were guided from the respective motors through fixed deflection units to control the motion of the oar for rowing application. At the other end of the oar, the handle of the oar was held by the user with both hands.

In the setup, the shortened oar was longitudinally fixed inside the oarlock with a clamp and bearing, which restrained the end-effector to move on a spherical surface. Therefore, the user could manipulate the oar in the three remaining rotational degrees of freedom. These three rotational oar movements were the horizontal oar angle θ, the vertical oar angle δ, and the longitudinal oar angle φ. Although the robot rendered forces in all three directions at the end-effector, the longitudinal forces were not transferred to the user due to the mechanical constraints of the oarlock. Rendered forces at the end-effector were haptically displayed to the user as torques along the horizontal oar angle θ and the vertical oar angle δ. The longitudinal oar angle φ was only controlled by the user.

The hardware configuration and rowing model application on our simulator was set up for portside sweep rowing. In sweep rowing, an even number of rowers are seated in the boat. Each rower holds a single oar at the oar handle with both hands. The haptic rendering of the rowing forces for this study was calculated for the portside and mirrored onto the bow side in the Matlab/Simulink® model to simulate a pair on the rowing simulator.

2.3. 3D Modeling of Rowing Forces

2.3.1. Sub-Phases of a Rowing Stroke

Rowing is a cyclic movement that is executed with the coordination of a complete set of body limbs to control an oar motion to propel the boat [32]. One rowing cycle, i.e., stroke, can be partitioned into four sub-phases, which features specific kinematic and kinetic characteristics. A cycle begins with the catch, followed by drive, release, and the recovery [1]. In the catch, the rower rapidly lifts the oar handle to insert the blade into the water and prepares for application of propulsive forces. During drive, the rower pulls the oar handle towards his/her body by a well-coordinated movement of legs, trunk, and arms, while the seat is moved towards the bow and the oar blade is moved through water with power. In the release, the oar handle is swiftly pushed down to remove the blade from the water and oar is feathered to reduce the air resistance [33]. In the recovery, when the blade is fully in the air, the rower flexes trunk and legs while extending the arms towards the stern of the boat to prepare for the next cycle [32].

2.3.2. Simulator Coordinates for the Rowing Models

To define the motion of the oar and resulting rowing forces, four different coordinate systems were defined. A boat-fixed coordinate system, i.e., $\chi_{Boat} = \left\{B_x,\ B_y,\ B_z\right\}$, was defined on the boat's center of gravity such that B_y was directed towards the stern and B_z upwards (Figure 2). An oar-fixed coordinate, i.e., $\chi_{Oar} = \left\{O_x,\ O_y,\ O_z\right\}$, was defined on the tip of the oar blade and was rotated with the blade movement. A special configuration of χ_{Oar} was defined as the initial oar coordinate system, i.e., $\chi_{Oar}^{initial} = \left\{O_x^i,\ O_y^i,\ O_z^i\right\}$, when the portside oar was in the initial configuration ($\theta = 0°, \delta = 0°,\ \varphi = 0°$) and perpendicular to the boat. Vertical (δ), longitudinal (φ), and horizontal (θ) rotations of the oar were the mathematically positive angles, i.e., defined in a counterclockwise (CCW) direction around $O_x^i,\ O_y^i,\ O_z^i$ axes, respectively. To calculate the forces acting against the oar blade resulting from the relative blade velocity, a stream coordinate system, i.e., $\chi_{Stream} = \left\{S_x,\ S_y,\ S_z\right\}$, was defined on the blade such that $S_y = -B_y$ and $S_z = B_z$.

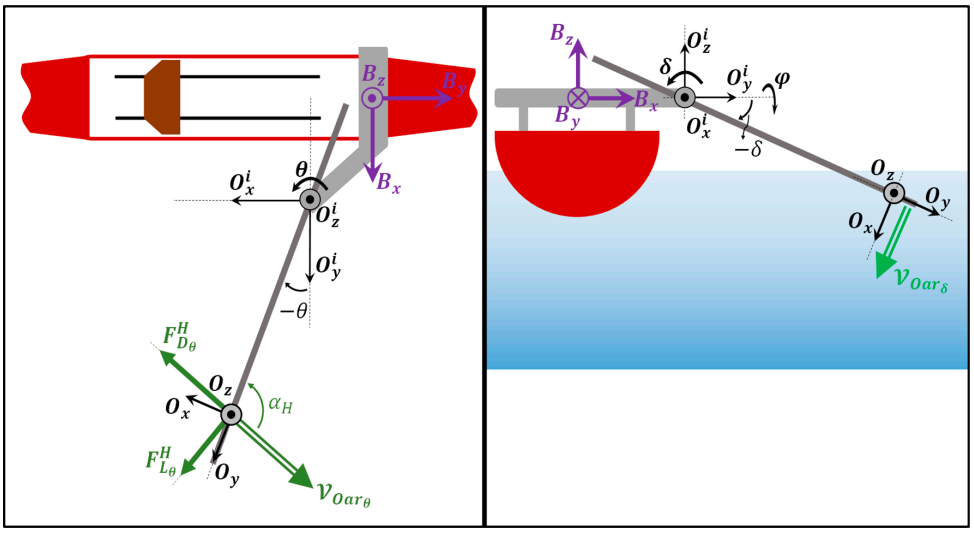

Figure 2. Coordinate systems and forces acting on the blade in the BIFC (binary blade immersion, fixed drag/lift coefficients) model. Forces due to horizontal oar movement are shown in the left pane (top view). the vertical force on the blade is shown in the right pane (back view of the boat).

Calculated rowing forces at the portside (right) oar blade were mirrored onto the bow side (left) blade, simulating identical rowers for a pair boat. As a result, the rotation of the simulated boat around the B_z-axis was assumed to be 0°, and the linear displacement of the boat was constrained to be along the B_y-axis for simplicity.

2.3.3. Description and Implementation of Base (1D) Models of Rowing for Blade–Water Interaction

Both rowing models presented in this paper were originally based on the modeling of drag and lift forces acting on a blade immersed into the water, which was provided by [34] as follows:

$$F_{Drag} = \frac{1}{2} C_D \rho A \left(\vec{V}_{o/w}\right)^2 \quad (1)$$

$$F_{Lift} = \frac{1}{2} C_L \rho A \left(\vec{V}_{o/w}\right)^2 \quad (2)$$

where $\rho = 1000 \frac{\text{kg}}{\text{m}^3}$ is the density of the water; $\vec{V}_{o/w}$ is the relative blade velocity between blade and water; A is the projected area of the blade (calculated perpendicular to the front of the blade); C_D and C_L are the angle of attack dependent dimensionless drag and lift force coefficients, respectively.

Both equations were based on an experiment in which the blade was inserted into the water tank and held fixed against a one dimensional (1D) incoming flow [34]. Thus, the relationship between the forces and the velocity of the blade was only considered on the horizontal plane.

An alternative version of the 1D rowing model described by Equations (1) and (2) was implemented for our rowing simulator by [30]. In the simplified version of the model, drag and lift forces acting on the oar blade in the horizontal plane were approximated as follows:

$$F_{Drag}^H = C_D(\alpha_H) \left(\vec{V}_{Oar_\theta}\right)^2 \quad (3)$$

$$F_{Lift}^H = C_L(\alpha_H) \left(\vec{V}_{Oar_\theta}\right)^2 \quad (4)$$

where

$$C_D(\alpha_H) = 2 C_L^{max} sin^2 \alpha_H \quad (5)$$

$$C_L(\alpha_H) = C_L^{max} sin2\alpha_H \tag{6}$$

and the angle of attack α_H was defined between the longitudinal axis of the oar and $\vec{V}_{Oar_\theta}$, i.e., the oar blade velocity that depends on the 1-DoF horizontal rotation of the oar (θ). C_L^{max} was calculated from the maximum value of lift coefficient C_L whose values were presented based on α_H in [34].

In principle, the force model presented in [34] with Equations (1) and (2), and the interaction forces calculated with Equations (3)–(6) are based on the assumption that the magnitude of drag and lift forces depend quadratically on the blade velocity. To our knowledge, Equations (3) and (4) were initially mentioned for drag and lift oar blade forces in [29] based on the authors' interpretation of the results from the experiments and force model presented in [35]. In [35], the authors empirically found an approximation of the drag C_D and lift C_L coefficients that depend on the angle of attack (Equations (5) and (6)), which were further considered for the modeling of rowing in [29,36], and calculation of the efficiency of rowing oars [37].

In [30], the oar blade was assumed to be squared (vertical with respect to water surface, i.e., $\varphi = 0°$), and the resultant force acting on the blade, i.e., F_θ, was only dependent on the horizontal (θ) movement of the oar.

$$F_\theta = \sqrt{\left(F_{Drag}^H\right)^2 + \left(F_{Lift}^H\right)^2} = 2C_L^{max}\left(\vec{V}_{Oar_\theta}\right)^2 sin\alpha_H \tag{7}$$

However, for a real rowing stroke, the resultant forces on a blade do not only depend on the horizontal rotation of the oar θ but also on the vertical δ and longitudinal rotation φ. Thus, two rowing models that incorporate three rotations of the oar are presented in the following sub-sections.

2.3.4. 3D rowing Model with Binary Blade Immersion and Fixed Drag/Lift Coefficients (BIFC)

In 2010, the 1D rowing model implemented by [30] was upgraded by [21] to a 3D rowing model, which incorporates the 3-DoF rotation of the oar (Figure 2). In [21], Equation (7) that was used for the θ angle-dependent forces was also applied to calculate the δ angle-dependent forces on the oar blade, i.e., F_δ, due to the vertical rotation (δ):

$$F_\delta = 2C_L^{max}\left(\vec{V}_{Oar_\delta}\right)^2 \tag{8}$$

where $V_{Oar_\delta} = l_{Oar}\dot{\delta}$, and l_{Oar} is the length of the oar.

The underlying assumption in Equation (8) was that the oar blade moved in the water with a feathered orientation (parallel with respect to the water surface, i.e., $\varphi = 90°$). No additional angle of attack was employed since the influence of an incoming stream in this direction was omitted. F_θ and F_δ were combined with the longitudinal oar angle (φ) to calculate the horizontal (F_{Oar}^H) and vertical (F_{Oar}^V) rowing forces based on three rotational angles of the oar blade as follows:

$$F_{Oar}^H = F_\theta cos^2\varphi + F_\delta \frac{sin2\varphi}{2} \tag{9}$$

$$F_{Oar}^V = F_\theta \frac{sin2\varphi}{2} + F_\delta sin^2\varphi \tag{10}$$

from which the overall oar blade force (F_{Oar}) could be calculated as

$$F_{Oar} = \sqrt{\left(F_{Oar}^H\right)^2 + \left(F_{Oar}^V\right)^2} = F_\theta cos\varphi + F_\delta sin\varphi. \tag{11}$$

Finally, to calculate the F_θ and F_δ, the value of the constant C_L^{max} was chosen as $42.25\frac{\mathrm{N}}{(\mathrm{m/s})^2}$ for a big blade area (A) of 0.13 m^2 based on the calculations in [29,37].

2.3.5. 3D Rowing Model with Linear Blade Immersion and Adjusted Drag/Lift Coefficients (LIAC)

In 2019, we developed a new 3D rowing model (linear blade immersion, adjusted drag/lift coefficients or LIAC), which was essentially based on Equations (1) and (2). In the model, F_{Drag} was defined in the opposite direction of the oar blade velocity while F_{Lift} was perpendicular to drag. During a continuous movement of the oar blade in the water, the magnitude and the direction of F_{Drag} and F_{Lift} change based on the values of drag (C_D) and lift (C_L) force coefficients, respectively. Furthermore, C_D and C_L were dependent on the instantaneous angle of attack. For the horizontal plane ($\mathcal{P}_{xy}$), we used a look-up table based on [34], which delivered the values of C_D and C_L depending on the calculated instantaneous angle of attack. Extending the model to the vertical plane ($\mathcal{P}_{yz}$), we employed a separate instantaneous angle of attack (Figure 3).

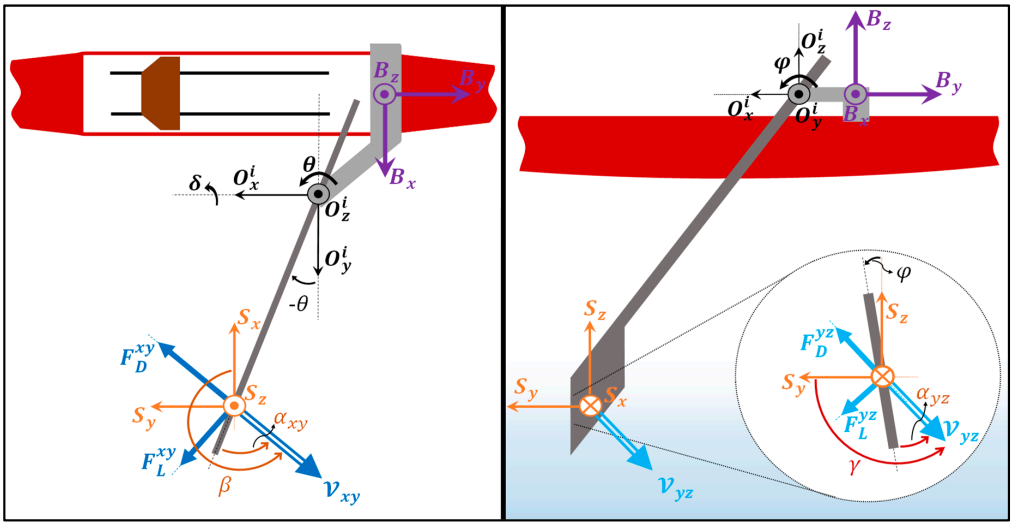

Figure 3. Coordinate systems and forces acting on the oar blade in the LIAC (linear blade immersion, adjusted drag/lift coefficients) model. Blade forces on the horizontal plane are shown in the left pane (top view). Blade forces on the vertical plane are shown in the right pane (side view of the boat). In the right pane, the enlarged circle shows the cross-section of the blade.

As a first step, the relative oar-blade velocity vector was defined in the boat-fixed coordinate system (χ_{Boat}) as $\vec{V}_{xyz} = \begin{bmatrix} V_{Oar_x} & V_{Oar_y} & V_{Oar_z} \end{bmatrix}^T$. To calculate the angles of attack for the oar blade motion in the horizontal ($\mathcal{P}_{xy}$) and vertical ($\mathcal{P}_{yz}$) planes, the projection of $\vec{V}_{xyz}$ vector onto these planes were described as $\vec{V}_{xy} = \begin{bmatrix} V_{Oar_x} & V_{Oar_y} \end{bmatrix}^T$ for the horizontal and $\vec{V}_{yz} = \begin{bmatrix} V_{Oar_y} & V_{Oar_z} \end{bmatrix}^T$ for the vertical planes.

According to the model presented in [34], the angle of attack used for the horizontal plane ($\mathcal{P}_{xy}$) was defined between the velocity of the oar blade ($\vec{V}_{xy}$) and the longitudinal (transverse) axis of the oar blade, yielding α_{xy}. Following a similar approach, the angle of attack used for the vertical plane ($\mathcal{P}_{yz}$) was defined between the $\vec{V}_{yz}$ component of the oar blade velocity and the cross section (vertical axis) of the blade, resulting in α_{yz}.

For the implementation of α_{xy} and α_{yz} calculations in a Matlab/Simulink® model, the following relationships were used (Figure 3):

$$\alpha_{xy} = \beta - \pi - \theta \tag{12}$$

$$\alpha_{yz} = \gamma - \frac{\pi}{2} + \varphi, \tag{13}$$

where β is an angle that is defined between $\vec{V}_{xy}$ and S_x in the horizontal plane (CCW around S_z), and γ is the angle between $\vec{V}_{yz}$ and the S_y (CCW around S_x).

Subsequently, drag and lift coefficients for both the horizontal and vertical forces were defined as $C_D^{xy} = f_D(\alpha_{xy})$, $C_L^{xy} = f_L(\alpha_{xy})$, $C_D^{yz} = f_D(\alpha_{yz})$, and $C_L^{yz} = f_L(\alpha_{yz})$, where the functions f_D and f_L were implemented as a look-up table based on the presented experimental values [34].

In the final step, the projected areas of the oar blade in the horizontal and vertical planes were calculated as follows:

$$A^{xy} = A_b p_{imm} cos\varphi \tag{14}$$

$$A^{yz} = A_b p_{imm} \tag{15}$$

where $A_b = 0.13\ m^2$ was chosen for a big blade used in sweep rowing. p_{imm} is the proportion of the oar blade in the water, which was calculated as

$$p_{imm} = \begin{cases} 0 & \text{for } \delta_{Surface} < \delta \\ \left| \frac{\delta - \delta_{Surface}}{\delta_{InWater} - \delta_{Surface}} \right| & \text{for } \delta_{InWater} < \delta \leq \delta_{Surface} \\ 1 & \text{for } \delta \leq \delta_{InWater} \end{cases} \tag{16}$$

where $\delta_{Surface}$ and $\delta_{InWater}$ are the vertical oar angles at which the tip of the blade touches the water surface and the blade is fully immersed in the water, respectively. Placement of Equation (16) in Equations (14) and (15) allowed for a smooth transition of forces between the drive and recovery.

For the calculation of A^{xy}, the projected area was assumed to be dependent only on the longitudinal oar angle φ since horizontal rotation of the oar θ was included in the calculation of horizontal angle of attack α_{xy}, which would update the magnitude of drag and lift coefficients according to the fluid dynamic model [34]. Moreover, for the calculation of A^{yz}, we assumed that the projected area would only depend on the immersion ratio of the blade since the vertical angle of attack α_{yz} was dependent on the longitudinal oar angle φ. In addition, a further trigonometric adjustment of the A^{yz} based on the horizontal angle θ resulted in low forces in the vertical plane during the pilot tests conducted on the simulator, which were not preferred by the experts. Therefore, we did not include any dependency of other oar angles to estimate A^{yz}.

Based on the previous calculations, the drag and lift forces of the model (LIAC) that resulted from the horizontal, vertical, and longitudinal rotation of the oar blade were calculated as follows:

$$F_{Drag}^{xy} = \frac{1}{2} C_D^{xy} \rho A^{xy} \left(\vec{V}_{xy} \right)^2 \tag{17}$$

$$F_{Lift}^{xy} = \frac{1}{2} C_L^{xy} \rho A^{xy} \left(\vec{V}_{xy} \right)^2 \tag{18}$$

$$F_{Drag}^{yz} = \frac{1}{2} C_D^{yz} \rho A^{yz} \left(\vec{V}_{yz} \right)^2 \tag{19}$$

$$F_{Lift}^{yz} = \frac{1}{2} C_L^{yz} \rho A^{yz} \left(\vec{V}_{yz} \right)^2. \tag{20}$$

To calculate the emerging horizontal ($F_H^{\chi_B}$) and vertical ($F_V^{\chi_B}$) plane forces acting on the oar blade in the boat-fixed coordinate system (χ_{Boat}), the drag and lift forces resulting from Equations (17)–(20) were transformed in the horizontal and vertical planes:

$$\vec{F}_H^{\chi_B} = {}^{Boat}\mathcal{R}_{Stream}(-\pi)\, {}^{Stream}\mathcal{R}_{xy}(\beta) \begin{bmatrix} F_{Drag}^{xy} & F_{Lift}^{xy} & 0 \end{bmatrix}^T \tag{21}$$

$$\vec{F}_V^{\chi_B} = {}^{Boat}\mathcal{R}_{Stream}(-\pi)\, {}^{Stream}\mathcal{R}_{yz}(\gamma) \begin{bmatrix} 0 & F_{Drag}^{yz} & F_{Lift}^{yz} \end{bmatrix}^T \tag{22}$$

where ${}^{Boat}\mathcal{R}_{Stream}(\theta_{rot} = -\pi)$ was used to define the χ_{Stream} in the boat-fixed coordinate system (χ_{Boat}), and ${}^{Stream}\mathcal{R}_{xy}(\beta)$ and ${}^{Stream}\mathcal{R}_{yz}(\gamma)$ were the transformation matrices in the horizontal and vertical planes, respectively.

According to the model presented by [34], the resulting plane forces of $\vec{F}_H^{\chi_B}$ and $\vec{F}_V^{\chi_B}$ define two distinct 2D models in the horizontal ($\mathcal{P}_{xy}$) and vertical ($\mathcal{P}_{yz}$) planes, respectively. In order to generate a 3D force (F_{Oar}) from two 2D models ($\vec{F}_H^{\chi_B}$ and $\vec{F}_V^{\chi_B}$), we employed a combination factor, which would satisfy the following constraints:

$$F_{Oar} = f\left(V_{xyz}^2\right)C_1 f\left(V_{xy}^2\right) + C_2 f\left(V_{xy}^2\right), \text{ where } C_1,\ C_2 \leq 1 \text{ and } C_1 + C_2 = 1. \tag{23}$$

C_1 and C_2 are the combination factors for the horizontal and vertical planes, respectively. The underlying assumption for the relationship in Equation (23) was that the blade forces calculated in each plane, i.e., $f\left(V_{xy}^2\right)$ and $f\left(V_{yz}^2\right)$, were dependent on the square of blade velocity that was projected onto the horizontal and vertical planes, respectively. Thus, to satisfy the relationship in Equation (23), C_1 and C_2 were defined as follows:

$$C_1 = \frac{V_{xy}^2}{V_{xy}^2 + V_{yz}^2} \tag{24}$$

$$C_2 = \frac{V_{yz}^2}{V_{xy}^2 + V_{yz}^2}. \tag{25}$$

Therefore, the 3D force resulting from Equations (23)–(25) was defined as

$$\vec{F}_{Oar} = C_1 \vec{F}_H^{\chi_B} + C_2 \vec{F}_V^{\chi_B}. \tag{26}$$

2.3.6. Rendering of Forces on the Rowing Simulator

To calculate the forces, rowing models were implemented in Matlab/Simulink® (r2013b, The MathWorks, Inc., Natick, MA, USA). To render the rowing forces at the end-effector, the actuators driving each rope were simultaneously controlled by the Matlab/Simulink® model running on an xPC-target at 1 kHz. The implemented rowing models required all oar angles (θ, δ, φ), the seat position x_s, and the seat acceleration $\ddot{x}_s$ as inputs to calculate the forces. Longitudinal oar angle φ and both of the seat parameters were measured with respective sensors in the instrumented boat. To retrieve the values of horizontal θ and vertical δ oar angles, the end-effector's position was initially calculated from the forward kinematics of the robot, i.e., change of rope lengths. Subsequently, a coordinate transformation was applied to the end-effector's position to calculate the horizontal θ and vertical δ oar angles. The longitudinal oar angle φ was measured with the potentiometers on the oar.

2.3.7. Control of Rope Tension Forces during Recovery

In the presented rowing models, the resistance forces resulting from air friction during recovery were not explicitly modeled. Instead, the resistance was provided with the residual forces acting at the oarlock, which results from tensioning the ropes of the tendon based parallel robot to control the translational motion of the end-effector, i.e., shortened oar.

A technical challenge regarding the use of a tendon based parallel robot is that rendering of high rowing forces at the end-effector due to rapid oar movements can result in unwanted transversal vibrations on the ropes and resonance on the robot. Since the vibrations mainly occur when the ropes are flexed, the stiffness control of the robot plays an important role in the haptic rendering of the rowing models on the simulator. Therefore, the natural (eigen) frequency of the system needs to be determined to understand the vibrational characteristics and assure the stiffness of the robot.

Assuming that the ropes are modeled as taut strings in our robot, the wave equation that governs the natural transversal vibration of the rope can be described as follows [38]:

$$\omega_n = \frac{n\pi}{l_i}\sqrt{\frac{\tau_i}{\zeta}} \tag{27}$$

where ω_n^i is the eigen frequency of the ith rope, n is nth frequency, l_i is the length of the ith rope, τ_i is the tension force on the ith rope, and ζ is the mass per unit rope length.

According to Equation (27), the natural frequency for transversal vibration of the rope is proportional to the square root of the rope tension and inversely dependent on the length of the rope. Confirming the relationship presented in Equation (27), three out of five ropes of the tendon based parallel robot are lengthened during catch-to-drive transition in the simulator, which reduces ω_n and thus results in increased transversal vibrations on the ropes. However, the vibration on the ropes can be suppressed if the eigenfrequency ω_n is increased. Although increasing the tension on the ropes would yield a stiffer tendon-based parallel robot, increased stiffness would also yield higher friction forces at the oarlock, which may cause unrealistically high resistive forces during recovery. Therefore, we could not use fixed, high tension forces on the ropes during whole rowing cycle to counteract the vibrations resulting from high rowing forces during catch and drive.

In the previous studies on the rowing simulator, the vibration problem could be suppressed by setting the minimum rope tension force (τ_{rope}^{min}) to a fixed value of 50 N , since the rendered forces at the end-effector were low due to the fact that body–arm rowing was used as the rowing task [24–27]. However, this minimum rope tension of 50 N yielded neither realistic recovery forces nor eliminated the transversal vibration issue for the rapid, full-body rowing movement. Therefore, we implemented a position-dependent τ_{rope}^{min} adjustment in the LIAC model. Three different thresholds for τ_{rope}^{min} were defined dependent on the vertical movement of the oar (δ) (Figure 4): τ_{rec}^{min} for the rope tension during recovery, $\tau_{transit}^{min}$ during catch and release, and τ_{drive}^{min} during drive.

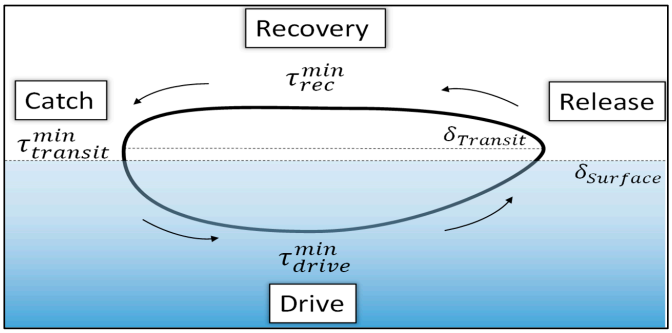

Figure 4. Illustration of the vertical oar rotation-dependent rope tension adjustment for the tendon based parallel robot. A typical rowing cycle is illustrated with the thick elliptic line. Four arrows show the direction of the oar blade within the cycle.

The linear adjustment of the rope tension forces were defined as follows:

$$\tau_{rope}^{min} = \begin{cases} \tau_{rec}^{min} & \text{for } \delta_{Transit} < \delta \\ \tau_{rec}^{min} + \left(\tau_{transit}^{min} - \tau_{rec}^{min}\right)\left(\frac{\delta_{Transit} - \delta}{\delta_{Transit} - \delta_{Surface}}\right) & \text{for } \delta_{Surface} < \delta \leq \delta_{Transit} \\ \tau_{transit}^{min} + p_{imm}\left(\tau_{drive}^{min} - \tau_{transit}^{min}\right) & \text{for } \delta \leq \delta_{Surface} \end{cases} \quad (28)$$

where $\delta_{Transit}$ is an empirically set value (1°) for the vertical oar angle above the simulated water surface. In Equation (28), initially set values for the parameters were $\tau_{transit}^{min} = 50$ N, $\tau_{drive}^{min} = 60$ N.

2.3.8. Configurable Parameters of LIAC for an Individualized Rowing Experience on the Simulator

A pilot study with three expert rowers, who were not included in main study, was conducted to assess and calibrate the newly developed LIAC model. The goal was to adjust the LIAC parameters, which would yield realistic forces for all sub-phases of the cycle and a corresponding boat velocity. Thus, we chose four parameters as follows that modulated the calculation of the forces: drag and lift adjustment coefficient (G_{dl}) for drive, curvature of the rowing blade (φ_{bias}) for catch and release, minimum rope tension force (τ_{rec}^{min}) for recovery, and boat drag coefficient (C_{Bdrag}) for the boat velocity.

For drive, three expert rowers reported that the resulting 3D model forces were greater than the forces felt during actual rowing. Thus, to calibrate the forces in the horizontal and vertical plane, we employed an additional gain, i.e., G_{dl}, for the adjustment of drag and lift coefficients:

$$C_{D'}^{xy} = G_{dl} f_D\left(\alpha_{xy}\right) \tag{29}$$

$$C_{L'}^{xy} = G_{dl} f_L\left(\alpha_{xy}\right) \tag{30}$$

$$C_{D'}^{yz} = G_{dl} f_D\left(\alpha_{yz}\right) \tag{31}$$

$$C_{L'}^{yz} = G_{dl} f_L\left(\alpha_{yz}\right) \tag{32}$$

where D' and L' subscripts define the adjusted drag and lift coefficients, which were replaced in Equations (17)–(20). In the end of the pilot test, G_{dl} was set to 0.35 by taking the average of the preferred gains reported by three expert rowers.

Another critique of the pilot test rowers was that the vertical forces during the air–water transition were low. Thus, we increased the vertical forces in the catch and release by introducing a bias angle, i.e., φ_{bias}, which was assumed to account for the lateral curvature of the rowing blade. Originally, the oar blade presented in the LIAC model was designed as a flat plate. Thus, introducing φ_{bias} yielded:

$$\varphi' = \varphi_{bias} + \varphi_{act} \tag{33}$$

where $\varphi_{act} = \varphi$ is the actual longitudinal rotation of the oar blade and φ' is the adjusted oar blade rotation used in the Matlab/Simulink® implementation. The initial value of φ_{bias} was set to 2°.

The minimum rope tension force in the tendon based parallel robot was adjusted for the rowing forces during recovery (τ_{rec}^{min}). Since τ_{rope}^{min} was set to a fixed value of 50 N for the overall cycle in the BIFC model, the initial value of τ_{rec}^{min} in the LIAC model was also set to 50 N for the recovery ($p_{imm} = 0$). All three rowers judged that the recovery force rendered by LIAC was unrealistically resistive; thus, an average value of 35 N was set for a smooth manipulation of the oar in the recovery.

Finally, pilot study rowers were asked to assess how well the perceived boat velocity matched the applied forces on the simulator. Based on the implementation of the rowing model, the boat velocity $\dot{y}_{boat}$, was dependent on the driving forces applied by the rowers on the oar blades ($F_{propulsion}$), inertia forces resulting from the movement of the rowers and the oar blades ($F_{inertia}$), and drag forces acting on the boat ($F_{BoatDrag}$).

$$m_{boat}\ddot{y}_{boat} = F_{Net} = F_{propulsion} - F_{inertia} - F_{BoatDrag} \tag{34}$$

where m_{boat} is the combined mass of rowers and the boat, and $\ddot{y}_{boat}$ is the acceleration of the boat in B_y-axis [28]. In Equation (34), $F_{BoatDrag}$ is calculated as in [29] as follows:

$$F_{BoatDrag} = C_{Bdrag}\left(\dot{y}_{boat}\right)^2 \tag{35}$$

According to Equation (34) and Equation (35), a modulation of C_{Bdrag} affected the acceleration and velocity of the boat, which also altered the calculated drag and lift forces from Equations (17)–(20).

The initial value of C_{Bdrag} in the LIAC model was set to 4.94 $\frac{\mathrm{N}}{(\mathrm{m/s})^2}$ based on the calculations for a pair type of boat in [30]. Pilot study rowers judged that the perceived boat acceleration and velocity (from the visual display as well as resulting forces on the blade) felt realistic for the given initial value. Although C_{Bdrag} was not further modulated in the pilot test but depended on the type and size of the boat [29], C_{Bdrag} was implemented in the model to be configurable by the rowers.

In the pilot test, we observed that the three rowers individually preferred slightly different values for the presented parameters, yielding a variety of rowing model settings. Indeed, rowers may differ in many aspects, e.g., anthropometric measures, technique, strength, accustomed water conditions (river, lake, or sea), preferred boat rigging, etc. Therefore, we decided to present the previously chosen

model parameters, i.e., G_{dl}, φ_{bias}, τ_{rec}^{min}, and C_{Bdrag}, also to the main study expert rowers as a means of adjusting the rowing model to their individual preferences. Initial values of all the model parameters for the main study were determined by taking the average of preferred values of pilot study rowers.

2.4. Experimental Protocol

The study consisted of two parts. In the first part, five training blocks were conducted (Figure 5). Each of the blocks served to focus on a different aspect of the rowing movement. In each block, both the BIFC and LIAC models were presented twice in a randomized manner, yielding four trials within the block. The order of model presentation was based on Latin square randomization. The order of models presented within a training block was different in each block for a participant. Participants were not explicitly informed about the number of different models or the order of the model presentation. They were only instructed to focus on the evaluation of the movement aspect in each of the trials within the training block. Each trial with the presented model lasted for two minutes unless the participant decided to finish the trial and rate the model on the questionnaire.

Trainings	Training 1					Training 2					Training 3					Training 4					Training 5					Training 6	
Trial	1	2	3	4		1	2	3	4		1	2	3	4		1	2	3	4		1	2	3	4		Conf.	Assm.
Model	BIFC	LIAC	LIAC	BIFC	Break	BIFC	LIAC	BIFC	LIAC	Break	LIAC	LIAC	BIFC	BIFC	Break	LIAC	BIFC	BIFC	LIAC	Break	BIFC	BIFC	LIAC	LIAC	Break	LIAC	
Questions	Q1 & Q2					Q3 & Q4					Q5 & Q6					Q7 & Q8					Q9 & Q10					Q1 to Q10	
Time [min]	2	2	2	2	2	2	2	2	2	2	2	2	2	2	2	2	2	2	2	2	2	2	2	2	5	5	5

Figure 5. Experimental protocol. Training 1 to 5 were run in the first part of the experiment. Training 6 was run in the second part. Conf. and Assm. stand for Configuration and Assessment, respectively.

Prior to the Training-1, participants were not provided with an additional familiarization trial with any of the models. After the completion of each training block (four trials), a two-minute break was given. The first part of the experiment ended with the completion of Training-5.

In the second part of the experiment, i.e., Training-6, the participant was only provided with the LIAC model. The participants were given a minute to get familiar (again) with the model. Thereafter, experts were free to configure the parameters that would adjust the relevant rowing forces within four to five minutes. Configuration of the LIAC model resulted in the 'individualized' model, i.e., IND. After the individual configuration, participants were given one more minute to row with the final set of configuration. Finally, participants were asked to re-evaluate each of the questions in the previously presented questionnaire. The final evaluation typically took five minutes.

2.5. Task

The goal of the experiment was to qualitatively assess the realism of the presented rowing models for different aspects of the rowing movement. Experts were asked to mainly perform a full-body rowing cycle by coordinating their body limbs. They could also try other types of movements, e.g., half-slide, body-arm, only-arms rowing, if they wanted. They were free to decide to row with a feathered, i.e., horizontal oar blade with respect to water surface, or a squared blade in the recovery. In Training-1 and Training-2, the rowers could also pause at a certain posture and insert the squared blade into virtual water or tap the feathered blade onto the virtual water surface.

Experts were instructed to consider the experiment on the rowing simulator as if it was a technical training on the water, i.e., rowing with low to medium stroke rates and 40–70% of maximum force application. To capture the realism of the rowing forces with both compared models, participants were not explicitly constrained to any stroke rate. However, due to our instruction, they were observed to row with a range between 12 and 28 strokes per minute.

In the first part of the study, expert rowers were asked to focus on specific aspects of the rowing movement. To familiarize the expert rowers with the simulator and compare the presented force models, rather secondary/inessential aspects of a rowing stroke were considered in the first two trainings. In Training-1, the focus was on the horizontal movement of the blade above the water surface. Rowers deliberately slid the feathered blade on the virtual water surface and tried braking with the squared blade, which is a typical move to stop the boat during water outings. In Training-2, vertical movement of the oar during air to water transition was considered. In this training, rowers tried to distinguish the vertical forces between the squared blade insertion into water and the feathered blade tapping onto water surface. In addition, they were requested to purposely square the oar blade near to the water surface to feel the vertical reaction forces from the water surface.

In Training-3, the focus was on the forces during drive and recovery. In Training-4, the focus was given to the oar blade forces during the air–water transition, i.e., catch and release. In Training-5, the rowers were asked to rate the overall perception of the rowing forces considering the whole cycle. Finally, they were asked to rate the realism of the flow (speed) of the visual scenario with respect to their stroke rate and the force they applied. Completion of every trial was followed by filling out a questionnaire.

In the second part of the study, i.e., Training-6, participants were asked which particular forces they would have liked to adjust for their individual preferences. Upon participants' requests, the study instructor set the respective parameters from the graphical user interface to update the relevant forces of the active rowing model. Participants were asked to give their verbal comments to fine tune the force model according to their rowing preferences. The configurable parameters were G_{dl}, φ_{bias}, τ_{rec}^{min}, and C_{Bdrag}. Once the participants were satisfied with the final individualized parameter settings, they were asked to assess the realism again.

2.6. Questionnaire

Two questionnaires with the same questions were prepared for both parts of the experiment. The questionnaires were used for the qualitative comparison of the rowing models not only to each other but also to the real rowing scenario on the water.

The questionnaires consisted of one page for each training block. On top of every page, the sub-goal of the training block and an 11-point Likert-scale was presented. On the Likert-scale, '0 = Not realistic at all', '5 = Moderate (Neutral)', and '10 = Feels like on the water' statements were inserted below the respective values. In the middle of the page, two questions were stated for every training aspect. A written instruction and an illustration were present to help participants understand the questions. The designs of both questionnaires were the same except the trial counts within the blocks. For the first part, i.e., Training-1 to 5, Questionnaire-1 included four boxes (one for each trial) for the rating input for two questions at the bottom of the page. For the second part, Questionnaire-2 included two boxes for two questions: an upper box for the mean value of LIAC that was calculated by the study instructor after the first part, and a lower box for the new evaluation rating input.

Both questionnaires were prepared in Microsoft Word. The questionnaires were displayed on a monitor, which was placed to the front-left side of the participant. Participants were also provided a keypad input device, which was placed on the left side of the boat, to rate the respective aspect of the rowing movement. Participants entered numerical values from zero to ten using the keypad to fill the question boxes for each trial. Participants were left alone in the simulator, and the study instructor waited outside to avoid affecting the experts by any means during the model evaluation.

2.7. Questionnaire Analysis (Statistics)

For the statistical analysis of questionnaire evaluation, Matlab® 2017a and RStudio (Integrated Development Environment for R, version 1.1.463, RStudio Team, 2018) software were used. Separate analyses were conducted for each part of the study since the goal in each analysis was different.

For the first part, to check if the compared base rowing models (BIFC, LIAC) significantly differed in terms of realism based on the qualitative evaluation with the Questionnaire-1, the following linear mixed effect (*lme*) model was used.

$$Q_i \sim BaseModel + (1 \mid Expert) \quad (lme\text{-}1)$$

where Q_i is the dependent variable that represents the questions in the questionnaire, and $i = 1, \ldots, 10$ is the index of each question. *BaseModel* is the categorically independent variable with two levels defined as BIFC and LIAC. Since the models were presented twice in the training blocks, both rating values were used for each rowing model for every Q_i in the *lme-1*. *Expert* is defined as the random factor since ratings in both models belonged to one participant.

A separate analysis was conducted for the effect of individualization in the second part of the study. To examine if the individual adjustment of forces yielded a significant improvement in the realism ratings in Questionnaire-2 for the rowing on the simulator, *lme-2* was constructed as follows.

$$Q_i \sim Configuration + (1 \mid Expert) \quad (lme\text{-}2)$$

where $Configuration$ is the categorical independent variable with two levels: the configurable base model, i.e., LIAC, and the individually configured model, i.e., IND. Since the configured model IND was rated once with Questionnaire-2 (after the individual adjustment in Training-6), the mean of two ratings for the LIAC model was retrieved from the first part of the study (Questionnaire-1) in *lme-2*.

For both lme models, "*lmerTest*" package was used to check the significance by retrieving the *p*-values. To check the main effect of *BaseModel* in *lme-1* and $Configuration$ in *lme-2*, the "*anova*" method was used. Normality of the residuals from both lme models were visually inspected using Q–Q plots. Resultant *p*-values below 0.05 were regarded to show significance. The *p*-values between 0.05 and 0.1 were considered as 'trending towards significance.

3. Results

For every participant, individual initial and final values of the LIAC model are listed in Table 1.

Table 1. Pre- and post-individualization values of the LIAC model parameters in Training 6.

Experts	Individually Configured Parameters of the LIAC Model							
	Gain for Drag and Lift Coefficient (G_{dl})		Minimum Rope Forces in Recovery (τ_{rec}^{min}) (N)		Gain for Boat Drag Coefficient (C_{Bdrag}) ($\frac{N}{(m/s)^2}$)		Oar Blade Curvature (φ_{bias}) (°)	
	Initial Value	Final Value	Initial Value	Final Value	Initial Value	Final Value	Initial Value	Final Value
E1	0.35	0.32	35	32	4.94	2.47	2	2
E2	0.35	0.38	35	35	4.94	4.94	2	0
E3	0.35	0.40	35	30	4.94	4.94	2	0
E4	0.35	0.37	35	30	4.94	6.18	2	0
E5	0.35	0.32	35	30	4.94	5.43	2	0
E6	0.35	0.32	35	30	4.94	4.94	2	0
E7	0.35	0.40	35	32	4.94	4.94	2	0
E8	0.35	0.35	35	30	4.94	5.19	2	0
E9	0.35	0.35	35	32	4.94	6.18	2	2
E10	0.35	0.35	35	32	4.94	4.45	2	0

3.1. Comparison of Base Rowing Models (BIFC vs. LIAC)

3.1.1. Aspect 1 and 2: Interaction between Oar Blade and Water Surface

For the horizontal and vertical blade movements above the water surface, the *lme-1* did not show any significant main effect of the *BaseModel* except the feathered blade sliding on the water surface (Table 2). For Question 1, LIAC was rated as more realistic than BIFC ($F_{BM}(1,\ 30) = 26.81$; $p < 0.001$) with a slightly above-medium value ($\mu^{Q1}_{LIAC} = 5.95$).

Table 2. Statistical results from lme-1 and lme-2 models for each question in the questionnaires.

Aspect of Rowing	Quest. Index	*lme-1*: *BaseModel* (BIFC vs. LIAC)		*lme-2*: *Configuration* (LIAC vs. IND)	
		Mean Rating of Models	**Main Effect of Group and *p*-Value**	**Mean Rating of Models**	**Main Effect of Group and *p*-Value**
A1	Q1	$\mu_{BIFC} = 4.05$ $\mu_{LIAC} = 5.95$	$F_{BM}(1,\ 30) = 26.81$ $p < 0.001$	$\mu_{LIAC} = 5.95$ $\mu_{IND} = 6.60$	$F_C(1,\ 10) = 6.01$ $p = 0.03$
	Q2	$\mu_{BIFC} = 6.15$ $\mu_{LIAC} = 5.85$	$F_{BM}(1,\ 30) = 0.57$ $p = 0.455$	$\mu_{LIAC} = 5.85$ $\mu_{IND} = 6.80$	$F_C(1,\ 10) = 5.56$ $p = 0.041$
A2	Q3	$\mu_{BIFC} = 6.00$ $\mu_{LIAC} = 5.75$	$F_{BM}(1,\ 30) = 0.23$ $p = 0.633$	$\mu_{LIAC} = 5.75$ $\mu_{IND} = 6.30$	$F_C(1,\ 10) = 4.86$ $p = 0.052.$
	Q4	$\mu_{BIFC} = 5.30$ $\mu_{LIAC} = 5.65$	$F_{BM}(1,\ 30) = 0.50$ $p = 0.484$	$\mu_{LIAC} = 5.65$ $\mu_{IND} = 6.40$	$F_C(1,\ 10) = 3.19$ $p = 0.104$
A3	Q5	$\mu_{BIFC} = 4.85$ $\mu_{LIAC} = 7.25$	$F_{BM}(1,\ 30) = 39.36$ $p < 0.001$	$\mu_{LIAC} = 7.25$ $\mu_{IND} = 8.20$	$F_C(1,\ 10) = 6.13$ $p = 0.032$
	Q6	$\mu_{BIFC} = 3.85$ $\mu_{LIAC} = 6.25$	$F_{BM}(1,\ 30) = 30.37$ $p < 0.001$	$\mu_{LIAC} = 6.25$ $\mu_{IND} = 8.00$	$F_C(1,\ 10) = 54.44$ $p < 0.001$
A4	Q7	$\mu_{BIFC} = 5.10$ $\mu_{LIAC} = 7.15$	$F_{BM}(1,\ 30) = 24.86$ $p < 0.001$	$\mu_{LIAC} = 7.15$ $\mu_{IND} = 8.00$	$F_C(1,\ 10) = 7.21$ $p = 0.023$
	Q8	$\mu_{BIFC} = 5.50$ $\mu_{LIAC} = 6.65$	$F_{BM}(1,\ 30) = 6.72$ $p = 0.015$	$\mu_{LIAC} = 6.65$ $\mu_{IND} = 7.80$	$F_C(1,\ 10) = 6.95$ $p = 0.025$
A5	Q9	$\mu_{BIFC} = 4.65$ $\mu_{LIAC} = 6.70$	$F_{BM}(1,\ 30) = 39.12$ $p < 0.001$	$\mu_{LIAC} = 6.70$ $\mu_{IND} = 7.90$	$F_C(1,\ 10) = 16.74$ $p = 0.002$
	Q10	$\mu_{BIFC} = 5.35$ $\mu_{LIAC} = 6.05$	$F_{BM}(1,\ 30) = 3.91$ $p = 0.057$	$\mu_{LIAC} = 6.05$ $\mu_{IND} = 6.40$	$F_C(1,\ 10) = 1.16$ $p = 0.306$

3.1.2. Aspect 3 and 4: Interaction of Oar Blade and Virtual Water during Sub-Phases of the Rowing Cycle

For all four sub-phases of the rowing cycle, *lme-1* revealed a significant main effect of the *BaseModel* (Question 5, 6, 7, and 8, Table 2). The LIAC was rated more realistic than BIFC for the drive (Q5: $F_{BM}(1,\ 30) = 39.36$; $p < 0.001$), recovery (Q6: $F_{BM}(1,\ 30) = 30.37$; $p < 0.001$), catch (Q7: $F_{BM}(1,\ 30) = 24.86$; $p < 0.001$), and release (Q8: $F_{BM}(1,\ 30) = 6.72$; $p = 0.015$). For all the sub-phases of the cycle, rating of LIAC was above medium. However, BIFC was rated below medium for drive and recovery and medium for the catch and release.

3.1.3. Aspect 5: Overall Realism of the Rowing Forces and Synchronized Flow of Visual Scenario

The *lme-1* revealed a significant main effect of *BaseModel* for the overall realism of the rowing forces and a trending main effect for the flow of visual scenario (Q10: $F_{BM}(1,\ 30) = 3.91$; $p = 0.057$). For Question 9, LIAC was rated more realistic than BIFC (Q9: $F_{BM}(1,\ 30) = 39.12$; $p < 0.001$) that was rated below medium. For Question 10, both models were rated with a slightly above-medium value (Table 2).

3.2. Effect of Individualized Configuration (LIAC vs. Individually Configured model (IND))

3.2.1. Aspect 1 and 2: Interaction between Oar Blade and Water Surface

The *lme-2* showed a main effect of *Configuration* for the horizontal movements of the oar blade above the water surface (Q1: $F_C(1, 10) = 6.01$; $p = 0.034$ and Q2: $F_C(1, 10) = 5.56$; $p = 0.041$) (Table 2). The realism rating value for the forces of oar blade sliding (Q1) increased by 11% compared to the LIAC model ($\mu_{IND}^{Q1} = 6.60$). Rating of the braking forces increased by 16%. Regarding the water surface interaction forces resulting from the vertical movement of the blade above surface, there was a trend for a main effect of the *Configuration* for the Question 3 (Q3: $F_C(1, 10) = 4.86$; $p = 0.052$). The rating value for the Question 3 increased by 10%. The *Configuration* did not yield any significance for the Question 4 although the rating value increased by 13%.

3.2.2. Aspect 3 and 4: Interaction of Oar Blade and Virtual Water during Sub-Phases of the Rowing Cycle

The *lme-2* showed a significant main effect of the *Configuration* for all four sub-phases of the rowing stroke (for Question 5, 6, 7, and 8, Table 2). Compared to base LIAC model, the configured LIAC model, i.e., IND, was rated more realistic for the drive (Q5: $F_C(1, 10) = 6.13$; $p = 0.032$), recovery (Q6: $F_C(1, 10) = 54.44$; $p < 0.001$), catch (Q7: $F_C(1, 10) = 7.21$; $p = 0.023$), and release (Q8: $F_C(1, 10) = 6.95$; $p = 0.025$). The rating values of the drive, recovery, catch, and release were increased by 13%, 28%, 12%, and 17%, respectively.

3.2.3. Aspect 5: Overall Realism of the Rowing Forces and Synchronized Flow of Visual Scenario

The *lme-2* revealed a main effect of *Configuration* only for the perception of overall rowing forces (Q9: $F_C(1, 10) = 16.74$; $p = 0.002$) (Table 2). The rating of Question 9 increased by 18% after individual configuration ($\mu_{IND}^{Q9} = 7.90$). Tuning of the rowing LIAC model did not significantly improve the perception of the visual scenario (Table 2), and the rating value increased by 6%.

4. Discussion

Robotic simulators provide an important environment for training of surgeons [39], pilots [40], motor learning of complex sports [41,42], and training of athletes for the performance improvement in real-life sports [22]. To benefit from simulator training in real-life tasks, simulators are required to realistically render the task aspects [43,44].

In this study, we propose a novel 3D rowing model to render the interaction forces between the oar blade and water for a rowing simulator. The implemented model was assessed by expert rowers in terms of the realism of the rendered rowing forces. The assessment of the realism was based on the subjective perception of the experts about how realistic the rowing forces were rendered. At first, two distinct 3D models were compared in numerous aspects of the rowing movement. We hypothesized that the new 3D rowing model would render the forces on the simulator more realistically than the previously implemented 3D model [21]. Secondly, we elaborated whether individualizing parameters of the new rowing model further increases the perceived realism of the interaction forces.

The consensus from the experts about the rowing simulator was that it provided a more realistic indoor training platform than any other rowing devices in the market due to incorporation of not only visual and auditory rendering of rowing aspects but also a realistic task force rendering with 3-DoF oar manipulation. Results from both parts of the study along with the impact of model parameters on the perceived realism are discussed in the following sub-sections.

4.1. Comparison of Two 3D Rowing Models (BIFC vs. LIAC)

Presented 3D rowing models that calculated drag and lift forces acting on the oar blade mainly differed in two parameters, i.e., use of angle of attack and the blade area in the water. In comparison to the BIFC model, the LIAC model not only incorporated the effect of angle of attack in horizontal plane

(α_{xy}) but also in the vertical plane (α_{yz}). In the LIAC model, the resultant drag and lift coefficients in horizontal and vertical planes were continuously adjusted according to the instantaneous angle of attack. On the contrary, a pre-determined value of C_L^{max} was used in the BIFC model for the forces in both planes and the vertical forces were not dependent on the angle of attack due to modeling assumptions. In addition, the BIFC model did not incorporate the effect of the oar-blade area in the water. However, forces from the LIAC model depended on the proportion of the blade area in the water.

We also investigated the effect of rope tension forces (τ_{rec}^{min}) on the rendering of recovery forces. In real rowing, rowers push the oar handle with a minimal force to move the oar from release to catch position during recovery. Thus, to provide a realistic feeling on the simulator during recovery, the rendered forces on the oar blade should be the lowest compared to other sub-phases of the rowing cycle. Therefore, we initially set the τ_{rec}^{min} value for the LIAC model to 35 N based on pilot study and compared to the τ_{rec}^{min} value of the BIFC model that was kept at 50 N .

4.1.1. Rowing Cycle and Sub-Phases

As hypothesized, the newly proposed 3D rowing LIAC model was rated as significantly more realistic than BIFC in drive (Q5), recovery (Q6), catch (Q7), release (Q8), and overall rowing cycle (Q9).

For drive, expert rowers mentioned that the rendered forces with LIAC were realistically resistive. The development of the force during early drive and the reduction of the force in the late drive was also judged as realistic. Experts also reported a smoother force increase and decrease in the catch and release, respectively. Inclusion of parameter p_{imm} in the blade area calculation accounted for a smooth transition of the oar blade during catch and release, which plays an important role in the exerted propulsion forces, continuity of the oar motion and elimination of unwanted decelerating blade drag forces [45].

On the other hand, the resistance provided by the BIFC model was reported to be low during the drive. It could be argued that a selection of a higher C_L^{max} value might have yielded a more realistically resistive force in drive. However, the force calculation in the BIFC model did not incorporate a parameter for the 'immersed blade area in the water' as in the case of LIAC. Thus, due to rapidly increased forces, the binary approach in the force modeling might have introduced a discrepancy during blade transition between air and water in the catch and release.

For recovery, superiority of the LIAC model over BIFC is not surprising because in the pilot tests, initially selected values of rope tension for LIAC ($\tau_{rec}^{min} = 50$ N) were also rated to be unrealistically high by three pilot experts. Nevertheless, we wanted to inspect and compare the overall ratings from main study expert rowers; thus, τ_{rec}^{min} forces in the BIFC model were maintained at 50 N . If we had lowered the τ_{rec}^{min} tension forces for the BIFC model, the observed significance regarding the realism of recovery forces of LIAC over BIFC would not have been found in our opinion.

4.1.2. Auxiliary Aspects of Rowing Movement

During actual rowing outings, rowers usually may need to stop the boat. Thus, rowers immerse the squared blade into the water to apply a braking motion. In the simulator, expert rowers were also asked to simulate a similar scenario, in which they would immerse the squared blade into water to decelerate the boat (Question 2). In this aspect, the perceived horizontal braking forces were not perceived differently for BIFC and LIAC. Some rowers described that braking forces were higher than they expected, which also decelerated the simulated boat more compared to an actual boat. This observation may be explained by the fact that effects of the Froude number and the turbulence were omitted in both models. In real blade–water interaction, the immersed area of the oar blade in the water may reduce the drag and lift force coefficients due to a change of the Froude number [46]. In addition, the turbulence was also shown to reduce the drag and lift coefficients in a computational study [47]. Thus, both effects should be implemented to yield more realistic interaction forces.

Another simplification was the geometrical modeling of the oar blade. In both rowing models BIFC and LIAC, the oar blade was initially modeled as a flat rectangular plate, i.e., the longitudinal and

lateral curvature of an original rowing blade [34] design was omitted. Based on the feedback from pilot study rowers regarding the vertical forces in the catch and release, φ_{bias} was implemented in LIAC to account for a simplified form of a lateral curvature of the blade. However, due to the simplified blade geometry, the contact area between the blade and water surface increased. Thus, rendered horizontal and vertical forces above the water surface were generally perceived as higher for the simulator than a real rowing scenario.

In real rowing, due to rolling of the boat to one side, rowers may sometimes unintentionally touch and slide the blade on the water surface when moving the oar from release to catch with a feathered blade. In the simulator, participants were asked to make a deliberate attempt to slide the feathered blades to simulate this scenario (Question 1). Rowers reported that the BIFC model rendered horizontal forces that decelerated the boat when the blade was slid parallel to the water surface (feathered oar). According to the mathematical modeling of BIFC, the ideal forces along the B_y-axis should be zero. However, the lack of curved blade design in addition to the binary modeling of the oar immersion, i.e., either fully in or fully out of the water, might have facilitated the blade immersion during the feathered position, which may have induced the reported braking forces.

Although LIAC was rated more realistic than BIFC for the horizontal forces resulting from feathered blade sliding, the mean rating was only above average ($\mu^{Q1}_{LIAC} = 5.95$). Braking forces were also reported for LIAC; however, the magnitude was perceived as lower in comparison to BIFC. The reason for the reported forces for LIAC was the introduction of φ_{bias}, whose initial value was set to 2° to simulate a rotated blade instead of a (laterally) flat one. Thus, especially a rapid movement towards the catch while sliding the blade on the water surface resulted small resistive forces.

For both rowing models, the lack of curved blade design also resulted in excessive vertical contact forces. Naturally, the more parallel a blade is oriented with respect to surface, the greater the vertical forces become acting on the blade due to the water contact. In Question 3 and 4, experts were asked to rate the realism of the vertical forces resulting from water surface contact for a range of oar blade rotation ($0° \leq \varphi \leq 90°$). For BIFC, experts judged that immersion or tapping with all φ orientations rendered higher vertical forces than real rowing. This observation may be attributed to the binary modeling of the oar immersion for the calculation of rowing forces. For LIAC, the squared blade insertion ($\varphi = 0°$) into water was reported to render realistically low vertical forces. However, tapping with the feathered blade ($\varphi = 90°$) rendered much higher vertical forces than the real rowing.

To encounter high vertical forces and ensure the safety of the users in the simulator, rendered vertical forces on the simulator were limited to 200 N in B_z-axis, which was mainly considered for the general rowing movement with the squared blade orientation. However, the selected force limit was perceived too high for rendering the vertical forces during feathered blade tapping onto the water surface. Thus, the vertical force limit should be lowered in the future implementation.

4.1.3. Visual Scenario

Although the velocity model proposed in [28] was not further modified for the first part of the study, the resultant velocity of the simulated boat might have differed due to the design of distinct force models. In the simulator, the visual scenario shown on the screens was updated according to the boat speed ($\dot{y}_{boat}$) that was calculated through Equation (34). The result from Question 10 showed that the LIAC model was only marginally better than BIFC for the realism of the visual scenario flow. However, ratings for both models were only above medium. Discussions with the experts revealed that the design of the visual scenario itself could be improved for a more realistic virtual reality immersion, e.g., placement of the virtual buoys, rendering of the regatta lane, etc. Thus, although the goal was to judge how well the visual scenario updated with respect to the performed stroke rate and applied force, the majority of the experts were distracted by certain features in the visual scene such as the visual rendering of blade and buoys.

4.2. Effect of Individualization on the Perceived Realism of a Rowing Simulator (LIAC vs. IND)

In the second part of the study, experts were presented with a pool of model parameters, which can be individually configured to attain the most preferred rowing scenario on the simulator. The configurable parameters were chosen as G_{dl}, φ_{bias}, τ_{rec}^{min}, and C_{Bdrag}.

Adjustment of G_{dl} was mainly proposed for the magnitude of the drag/lift forces in drive, catch and release; however, it also influenced the forces resulting from blade and water surface interaction. Seven out of ten rowers preferred a different value of G_{dl} (range: 0.32–0.40, Table 1) after testing the simulator with a variety of G_{dl} settings. The modulation of G_{dl} resulted in an analogous effect as the damper setting on an ergometer. Four out of five male rowers preferred a higher setting while three females settled on a lower setting than the initial value of 0.35.

The bias factor φ_{bias} was originally introduced to modulate the vertical forces during catch and release. Change of φ_{bias} affected the value of the projected blade area for both the horizontal and vertical plane forces. In Training-6, eight out of ten rowers did not prefer the previously introduced φ_{bias} for rendering higher vertical forces in the catch and release (Table 1). φ_{bias} was set back to 0° for these participants. Thus, while rowing with a squared blade, decreased value of φ_{bias} resulted in lower vertical forces.

Configuration of τ_{rec}^{min} was offered for the resistive forces during recovery. Overall, nine experts decided to configure the rope tension forces (τ_{rec}^{min}) to a lower value than the initial setting (initial: 35 N , range after configuration: 30–35 N, Table 1).

Finally, modification of C_{Bdrag} was proposed to alter the boat velocity and thus, the resultant drag forces. Originally, the parametrization of C_{Bdrag} was suggested during pilot test to account for different rowing boat types since the rowers may be more familiar with training on a certain type of boat. However, during the main study, some rowers criticized the decelerating drag forces acting on the blade at the water entry and exit. The decelerating drag forces were caused by the stream velocity (negative of calculated boat velocity), which acted in the $+B_y$-direction. Therefore, C_{Bdrag} was the only relevant configurable parameter available to us, which could influence the magnitude of decelerating drag forces through boat velocity. For example, increment of C_{Bdrag} resulted in a reduced boat velocity (Equation (34)), which reduced the braking forces in $+B_y$-direction at the water entry and exit.

4.2.1. Rowing Cycle and Sub-Phases

The individualization of the model parameters significantly improved the perceived realism of forces in drive, recovery, catch, release, and overall rowing cycle.

For drive, individualization of G_{dl} was the key factor for the increased realism of resistive forces in the water. All participants except one were content with the magnitude of resistance, the peak force, and the change of forces in the water ($\mu_{IND}^{Q5} = 8.20$). One participant reported that he felt constrained by the simulator when he tried to apply high propelling forces. This observation can be attributed to the fact that the rendering of the horizontal forces was also bounded with a safety limit of 450 N in the B_y-axis. For the experiment, rowers were instructed to row with 40–70% of maximum force application and within low to medium stroke rates to assess the general capability of the simulator. Since the participants were not explicitly informed about the safety limit, their expected force peak was not rendered for the rowers who applied higher propelling forces. Therefore, the simulator will be tested in future for a higher force rendering to account for higher propelling forces by the rowers.

For recovery, individualization of rope tension forces significantly improved the perceived realism of forces ($\mu_{IND}^{Q6} = 8.00$). Although a setting of 30 N rendered reduced recovery forces, some rowers preferred to experience the slight resistance, referring to the real rowing in a windy weather. Few rowers actually preferred to set even lower values than 30 N for τ_{rec}^{min} stating that the residual resistance could still be perceived. However, due to design criteria of a tendon based parallel robot, the ropes must always be under tension to control the end-effector movement. Additionally, the selected value for τ_{rec}^{min} should ensure a smooth transition from τ_{rec}^{min} to τ_{drive}^{min} without causing disruptive tension–force jumps on the ropes. Thus, for control and safety reasons the lowest limit of τ_{rec}^{min} was set to 30 N . Nevertheless,

the selected value was based on the initial trials on the simulator, and further experiments may yield a safe and less resistive τ_{rec}^{min} tension forces on the ropes.

Overall, individualization of φ_{bias}, G_{dl}, and C_{Bdrag} led to significant improvement in the ratings of catch and release ($\mu_{IND}^{Q7} = 8.00$, $\mu_{IND}^{Q8} = 7.80$). A final setting of $\varphi_{bias} = 0°$ was mainly reported to have rendered more realistic vertical forces during blade transition. In addition, four rowers who preferred a higher value of C_{Bdrag} judged that the increment encountered the previously criticized high decelerating drag forces at the initial and final blade contact with the water. However, other rowers who preferred the same or lower C_{Bdrag} values notified us that lower braking forces would be preferred. If the rendering of high braking forces at the water entry and exit had been reported in the pilot study, implementation of Froude number and turbulence effects to reduce the drag/lift coefficients might have been a more convenient approach than adjusting C_{Bdrag}.

4.2.2. Auxiliary Aspects of Rowing Movement

Overall, the individualization of the G_{dl}, φ_{bias}, and C_{Bdrag} significantly improved the perceived realism of the horizontal forces resulting from blade contact with the water. However, due to previously presented blade modeling simplifications and safety limits, the increment on the rating of vertical contact forces were insignificant.

Setting φ_{bias} back to 0°, as preferred by the majority of experts, led to a significant increase in the realism perception of the horizontal forces when sliding the blade (Question 1). Although experts were more consistent with the rating values for the configured model IND, on average the realism was only above average ($\mu_{IND}^{Q1} = 6.60$). This result may be explained with the lack of longitudinal curvature in the modeling of the blade surface. In a real rowing case, inserting a feathered blade into the water requires a deliberate attempt to push the oar handle upwards due to the curved design of the blade. However, due to the flat-plate modeling of the oar blade, rowers were still able to insert the feathered blade into the simulated water, which produced slight decelerating drag forces.

Significant improvement in the realism of the braking forces (in Question 2) may be attributed to the rowers who settled on a lower value for G_{dl} and/or C_{Bdrag} during individualization, which reduced the high braking forces encountered in the first part of the study. Nonetheless, the average rating for the realism of braking forces were only above average ($\mu_{IND}^{Q2} = 6.80$). The result can be attributed to the rowers, who preferred higher values for the both drag coefficients. Thus, the previously reported issue regarding the excessive braking forces was repeated.

For the vertical forces acting on the blade due to contact with water surface, individualization of G_{dl} only resulted in a marginally significant increment ($\mu_{IND}^{Q3} = 6.30$). The majority of the rowers, who preferred $\varphi_{bias} = 0°$, mentioned that the minor reduction of the vertical forces were more realistic compared to $\varphi_{bias} = 2°$. However, for the tapping with feathered blade onto the water surface, previously reported unrealistically high vertical force rendering was stated again in Question 3 and 4. Repetition of the issue was an expected outcome due to the lack of realistic blade modeling and used safety limit of 200 N . in B_z-axis, which were not among the configurable parameters.

4.2.3. Visual Scenario

During model individualization in Training-6, rowers were instructed to focus on the configuration of the rowing forces. When the participants settled on their preferred rowing forces on the simulator, they were asked to evaluate the realism of the simulated boat speed from the visual scenario displayed on the screens.

Results showed that although a slight improvement was observed in the rating, force model configuration failed to significantly improve the perception regarding the flow of visual scenario ($\mu_{IND}^{Q9} = 6.40$). Based on the rowers' feedback, the design of the visual scenario was the main factor that might have distracted the experts. Rowers especially stated that the virtual buoy placement in the visual scenario was perceived narrower than a normal regatta lane, which prevented them from comparing the simulator to the real life rowing. A few rowers also mentioned that they did not have

adequate experience on a pair (2-) boat. These rowers reported that they were accustomed to rowing in bigger boats such as four (4-) and eight (8+), which are faster than a pair (2-) according to regatta results [48]. Thus, the resultant simulated boat velocity might have been slower for these rowers.

4.3. Practical Implications

To experience a realistic rowing training scenario in a simulator, expert rowers demand well-designed and synchronized rendering of visual, auditory, and haptic aspects of the task. In our simulator, forces rendered by the implemented rowing model and the synchronous rendering of visual and auditory displays were generally found to be realistic by the expert rowers. However, simplifications during modeling and technical limitations of the hardware setup might have led to perception of unnatural forces or unrealistic auditory and visual features, which may have confounded the overall realism of rowing scenario in the simulator. Therefore, in cases where residual technical problems cannot be readily resolved due to practical or safety reasons, individualization of the model parameters might be an appropriate approach to maintain or increase the perceived realism of the simulator.

Indeed, in our study, individualization of the model parameters was observed to yield a significant improvement in the acceptance of training on the simulator. Thus, expert rowers were also asked which other parameters of the rowing model and features to enhance the indoor training they would prefer to have on the simulator.

The majority of the experts proposed the parametrization of the inboard and outboard length of the oar, which could be virtually configured based on the rigging preferences of the rower. In real rowing, the preferred inboard and outboard oar lengths are usually found after a trial and testing process in the trainings. The required length of the oar also needs to be adjusted for the weather conditions. Thus, our rowing simulator can provide an easy and fast rigging within a training session.

In addition, expert rowers were interested in visualizing the errors related to the kinematic and dynamic outcomes of their rowing strokes in the simulator. Although commercial products, which can provide propulsion forces and oar kinematics while rowing on a boat, are available, these devices are not yet capable of providing feedback about the resulting errors, i.e., difference between desired and actual performance [49,50]. Therefore, as previously studied with beginner rowers, three modalities rendered on the rowing simulator could also be used to present feedback to the expert rowers for performance enhancement [26,51,52].

Some expert rowers were also interested in the visual display of an ‘opponent boat’, against which the rower in the simulator can train or race to simulate a regatta scenario. According to this idea, the ‘opponent boat’ could be set to propel with a desired speed setting, and the rower in the simulator could train to match the set goals for the training. Therefore, realistic rendering of the rowing forces can further be employed to augment the simulator to train professional athletes [53].

Finally, thanks to the achieved haptic realism of a sweep rowing application, potential sources of injuries associated with the asymmetries unique to the sweep rowing can be systematically assessed on our virtual reality simulator [54–56].

4.4. Limitations

Although rolling motion is important in real rowing for training the balance of the boat, the actuation of rolling angle on the rowing simulator was not included for safety reasons and controlling issues of the tendon based parallel robot. As reported by the participants, fixation of the boat for rolling motion helped to focus more on the relevant features and forces of rowing motion, although on the other hand, it lessened the overall haptic realism of the simulator compared to a training with an actual rowing boat on water. This technical drawback may be counteracted by introducing augmented reality headsets that can combine real life view of the rowing simulator and virtual rendering of boat rolling on the simulated water.

Another technical limitation was the use of fixed oarlock height for all the participants. The oarlock height was not adjustable due to the attachment of the end-effector (shortened oar) with the tendon based parallel robot. To operate the simulator, the oar and the boat had to be kept at a pre-defined position for the calibration of rope tension forces in the tendon based parallel robot. Since changing the end-effector position (by changing oarlock height) affected the calibration process of the robot, the oarlock was not adjusted. Therefore, some participants could not row with their most preferred rigging setting, which might also reflect the overall rating of the force models.

Due to the scope of the study, assessment of the realism of the rendered rowing forces were based on the subjective perception of the expert rowers. Therefore, future studies are required to objectively assess the realism by comparing the rendered rowing forces on the simulator to the on-water force measurements.

5. Conclusions

In this study, we presented a new rowing model that computed the blade–water interaction forces based on three rotational movements of the oar and implemented the model in our rowing simulator. We asked expert rowers to qualitatively assess the realism of the resulting forces for various rowing aspects on our rowing simulator. Based on the evaluation of experts, we found that the newly proposed 3D rowing model, which incorporated continuously adjusted drag/lift coefficients and immersed area of the blade, was highly realistic for the sub-phases and overall rowing cycle. We also showed that when the rowing model parameters were configured according to individual preferences of expert rowers, the perceived realism significantly increased.

The implementation of the proposed 3D rowing model for the haptics and the audiovisual rendering of the rowing scenario on the virtual reality simulator provide a realistic indoor training opportunity to rowers with different expertise levels. Thanks to the parametric design of the model and the real-time operation of the simulator, rowers and coaches can choose and immediately test the inquired settings to increase the rowing performance. The pool of configurable parameters can easily be extended to include the boat and oar rigging, which may further help rowers to find their most preferred rowing configuration in a boat. Therefore, our rowing simulator does not only provide an indoor rowing training facility but also a platform, which assists rowers and coaches to find the most optimal rowing settings.

Author Contributions: E.B. contributed to the rowing model development, vibration control of the parallel robot, experimental protocol design, questionnaire preparation, conducting of the experiments, data acquisition, and statistical analysis and prepared the manuscript. P.B. conducted his MSc. semester thesis, in which he contributed to the rowing model development and vibration control of the parallel robot. N.G. and G.R. contributed to the rowing model conceptualization, solution of technical problems encountered during model development, and they revised the manuscript. P.W. participated in the experimental protocol design and questionnaire preparation, contributed to discussion of the statistical analysis results, and revised the manuscript. All authors have read and agreed to the published version of the manuscript.

Funding: This research received no external funding.

Acknowledgments: We would like to thank the rowers who took part in testing the models during the development phase and pilot study. We also express our gratitude to Michael Herold-Nadig for his technical support and safety testing of the rowing simulator.

Conflicts of Interest: The authors declare no conflict of interest.

References

1. Smith, R.M.; Loschner, C. Biomechanics feedback for rowing. *J. Sports Sci.* **2002**, *20*, 783–791. [CrossRef] [PubMed]
2. Warmenhoven, J.; Cobley, S.; Draper, C.; Smith, R. Over 50 Years of Researching Force Profiles in Rowing: What Do We Know? *Sports Med.* **2018**, *48*, 2703–2714. [CrossRef] [PubMed]
3. Hawkins, D. A new instrumentation system for training rowers. *J. Biomech.* **2000**, *33*, 241–245. [CrossRef]

4. Hofmijster, M.J.; Landman, E.H.; Smith, R.M.; Van Soest, A.J. Effect of stroke rate on the distribution of net mechanical power in rowing. *J. Sports Sci.* **2007**, *25*, 403–411. [CrossRef]
5. Nolte, V. *Rowing Faster*, 2nd ed.; Human Kinetics: Champaign, IL, USA, 2011.
6. Schmidt, R.A.; Wrisberg, C.A. *Motor Learning and Performance: A Situation-Based Learning Approach*; Human kinetics: Champaign, IL, USA, 2008.
7. Kleshnev, V.; Nolte, V. Learning from racing. In *Rowing Faster*; Human Kinetics: Champaign, IL, USA, 2011.
8. Soper, C.; Hume, P.A. Towards an ideal rowing technique for performance. *Sports Med.* **2004**, *34*, 825–848. [CrossRef]
9. A Brief History of Rowing Machines. Available online: www.allrowers.com/history-of-rowing-machines.html (accessed on 21 December 2019).
10. Stettler, D. Improvement of oar water interactions in the M3-rowing simulator. Bachelor's Thesis, Swiss Federal Institute of Technology (ETH) Zurich, Zurich, Switzerland, June 2014.
11. Indoor Rowing Tanks. Available online: www.durhamboat.com/rowing-tanks/ (accessed on 22 December 2019).
12. Air vs. Magnetic Rowing Machine: What Is the Difference? Available online: www.rowingmachineking.com/air-vs-magnetic-rowing-machine-difference/ (accessed on 22 December 2019).
13. Kleshnev, V. Comparison of on-water rowing with its simulation on Concept2 and Rowperfect machines. In Proceedings of the ISBS-Conference Proceedings Archive, Beijing, China, 22–27 August 2005.
14. Indoor Sculler. Available online: www.rowperfect.com.au/ (accessed on 22 December 2019).
15. Dynamic Indoor Rower for Athletes & Teams. Available online: www.concept2.com/indoor-rowers/dynamic (accessed on 22 December 2019).
16. Rowing Innovations. Available online: www.rowinginnovations.com/swingulator-sweep-trainer/ (accessed on 22 December 2019).
17. Coffey Corporation. Available online: coffeycorporation.com/SimulatOar.php (accessed on 22 December 2019).
18. Biorower. Available online: www.biorower.com/ (accessed on 22 December 2019).
19. Filippeschi, A.; Ruffaldi, E. Boat dynamics and force rendering models for the sprint system. *IEEE Trans. Hum. Mach. Syst.* **2013**, *43*, 631–642. [CrossRef]
20. Ruffaldi, E.; Filippeschi, A. Structuring a virtual environment for sport training: A case study on rowing technique. *Robot. Auton. Syst.* **2013**, *61*, 390–397. [CrossRef]
21. Rauter, G.; von Zitzewitz, J.; Duschau-Wicke, A.; Vallery, H.; Riener, R. A tendon-based parallel robot applied to motor learning in sports. In Proceedings of the 2010 3rd IEEE RAS & EMBS International Conference on Biomedical Robotics and Biomechatronics, Tokyo, Japan, 26–29 September 2010; pp. 82–87.
22. Rauter, G.; Sigrist, R.; Koch, C.; Crivelli, F.; van Raai, M.; Riener, R.; Wolf, P. Transfer of complex skill learning from virtual to real rowing. *PLoS ONE* **2013**, *8*, e82145. [CrossRef]
23. M3 Rowing Simulator. Available online: www.rowing.ethz.ch/ (accessed on 22 December 2019).
24. Basalp, E.; Gerig, N.; Marchal-Crespo, L.; Sigrist, R.; Riener, R.; Wolf, P. Visual augmentation of spatiotemporal errors in a rowing task. In Proceedings of the Human Movement and Technology: Book of abstracts-11th Joint Conference on Motor Control & Learning, Biomechanics & Training, Darmstadt, Germany, 28–30 September 2016.
25. Gerig, N.; Basalp, E.; Sigrist, R.; Riener, R.; Wolf, P. Visual error amplification showed no benefit for non-naïve subjects in trunk-arm rowing. *Curr. Issues Sport Sci. (CISS)* **2019**, *3*. [CrossRef]
26. Rauter, G.; Gerig, N.; Sigrist, R.; Riener, R.; Wolf, P. When a robot teaches humans: Automated feedback selection accelerates motor learning. *Sci. Robot.* **2019**, *4*, eaav1560. [CrossRef]
27. Basalp, E.; Marchal-Crespo, L.; Rauter, G.; Riener, R.; Wolf, P. Rowing simulator modulates water density to foster motor learning. *Front. Robot. AI* **2019**, *6*, 74. [CrossRef]
28. Rauter, G. Enhancing Robot-Assisted Motor Learning by a Virtual Trainer. Ph.D. Thesis, Swiss Federal Institute of Technology (ETH) Zurich, Zurich, Switzerland, 2013.
29. Cabrera, D.; Ruina, A.; Kleshnev, V. A simple 1+ dimensional model of rowing mimics observed forces and motions. *Hum. Mov. Sci.* **2006**, *25*, 192–220. [CrossRef] [PubMed]
30. von Zitzewitz, J.; Wolf, P.; Novaković, V.; Wellner, M.; Rauter, G.; Brunschweiler, A.; Riener, R. Real-time rowing simulator with multimodal feedback. *Sports Technol.* **2008**, *1*, 257–266. [CrossRef]

31. Zitzewitz, J.v.; Rauter, G.; Steiner, R.; Brunschweiler, A.; Riener, R. A versatile wire robot concept as a haptic interface for sport simulation. In Proceedings of the 2009 IEEE International Conference on Robotics and Automation, Kobe, Japan, 12–17 May 2009; pp. 313–318.
32. Dawson, R.; Lockwood, R.; Wilson, J.; Freeman, G. The rowing cycle: Sources of variance and invariance in ergometer and on-the-water performance. *J. Mot. Behav.* **1998**, *30*, 33–43. [CrossRef] [PubMed]
33. Tessendorf, B.; Gravenhorst, F.; Arnrich, B.; Tröster, G. An imu-based sensor network to continuously monitor rowing technique on the water. In Proceedings of the 2011 Seventh International Conference on Intelligent Sensors, Sensor Networks and Information Processing, Adelaide, Australia, 6–9 December 2011; pp. 253–258.
34. Caplan, N.; Gardner, T.N. A fluid dynamic investigation of the Big Blade and Macon oar blade designs in rowing propulsion. *J. Sports Sci.* **2007**, *25*, 643–650. [CrossRef]
35. Wang, Z.J.; Birch, J.M.; Dickinson, M.H. Unsteady forces and flows in low Reynolds number hovering flight: Two-dimensional computations vs robotic wing experiments. *J. Exp. Biol.* **2004**, *207*, 449–460. [CrossRef]
36. On Rowing. Available online: home.hccnet.nl/m.holst/RoeiWeb.html (accessed on 14 December 2019).
37. Cabrera, D.; Ruina, A. Propulsive efficiency of rowing oars. *J. Appl. Biomech.* **2006**.
38. Diao, X.; Ma, O. Vibration analysis of cable-driven parallel manipulators. *Multibody Syst. Dyn.* **2009**, *21*, 347–360. [CrossRef]
39. Enayati, N.; Okamura, A.M.; Mariani, A.; Pellegrini, E.; Coad, M.M.; Ferrigno, G.; De Momi, E. Robotic assistance-as-needed for enhanced visuomotor learning in surgical robotics training: An experimental study. In Proceedings of the 2018 IEEE International Conference on Robotics and Automation (ICRA), Brisbane, Australia, 21–25 May 2018; pp. 6631–6636.
40. De Winter, J.C.; Dodou, D.; Mulder, M. Training effectiveness of whole body flight simulator motion: A comprehensive meta-analysis. *Int. J. Aviat. Psychol.* **2012**, *22*, 164–183. [CrossRef]
41. Marchal-Crespo, L.; van Raai, M.; Rauter, G.; Wolf, P.; Riener, R. The effect of haptic guidance and visual feedback on learning a complex tennis task. *Exp. Brain Res.* **2013**, *231*, 277–291. [CrossRef]
42. Rauter, G.; Sigrist, R.; Riener, R.; Wolf, P. Learning of temporal and spatial movement aspects: A comparison of four types of haptic control and concurrent visual feedback. *IEEE Trans. Haptics* **2015**, *8*, 421–433. [CrossRef] [PubMed]
43. Gopher, D. Skill training in multimodal virtual environments. *Work* **2012**, *41*, 2284–2287. [CrossRef] [PubMed]
44. Miles, H.C.; Pop, S.R.; Watt, S.J.; Lawrence, G.P.; John, N.W. A review of virtual environments for training in ball sports. *Comput. Graph.* **2012**, *36*, 714–726. [CrossRef]
45. Rowing Technique for Coaches—Catch, Drive, Release and Recovery. Available online: http://rowingact.org.au/former%20website/SDO/TECHNIQUE_1.html (accessed on 19 December 2019).
46. Macrossan, M.N.; Kamphorst, M. *Computational Study of the Froude Number Effects on the Flow around a Rowing Blade*; Department of Mechanical Engineering Report, University of Queensland: Queensland, Australia, October 2009.
47. Coppel, A.L. A Computational Fluid Dynamic Investigation of Rowing Oar Blades. Ph.D. Thesis, University of Birmingham, Edgbaston, Birmingham, UK, 2010.
48. 2019 World Rowing Championships. Available online: http://www.worldrowing.com/events/2019-world-rowing-championships/schedule-results (accessed on 19 December 2019).
49. OARS - smartOar. Available online: https://www.smartoar.com/oars/ (accessed on 20 December 2019).
50. Biorow Sensors and Electronics. Available online: http://biorow.com/products/biorow_sensors/ (accessed on 19 December 2019).
51. Sigrist, R.; Rauter, G.; Riener, R.; Wolf, P. Terminal feedback outperforms concurrent visual, auditory, and haptic feedback in learning a complex rowing-type task. *J. Mot. Behav.* **2013**, *45*, 455–472. [CrossRef]
52. Sigrist, R.; Rauter, G.; Marchal-Crespo, L.; Riener, R.; Wolf, P. Sonification and haptic feedback in addition to visual feedback enhances complex motor task learning. *Exp. Brain Res.* **2015**, *233*, 909–925. [CrossRef]
53. Wellner, M.; Sigrist, R.; von Zitzewitz, J.; Wolf, P.; Riener, R. Does a virtual audience influence rowing? *Proc. Inst. Mech. Eng. P J. Sports Eng. Technol.* **2010**, *224*, 117–128. [CrossRef]
54. Readi, N.; Rosso, V.; Rainoldi, A.; Vieira, T. Do sweep rowers symmetrically activate their low back muscles during indoor rowing? *Scand. J. Med. Sci. Sports* **2015**, *25*, e339–e352. [CrossRef]

55. Fohanno, V.; Nordez, A.; Smith, R.; Colloud, F. Asymmetry in elite rowers: Effect of ergometer design and stroke rate. *Sports Biomech.* **2015**, *14*, 310–322. [CrossRef]
56. Parkin, S.; Nowicky, A.V.; Rutherford, O.M.; McGregor, A.H. Do oarsmen have asymmetries in the strength of their back and leg muscles? *J. Sports Sci.* **2001**, *19*, 521–526. [CrossRef]